First-principles theory of the coherency strain, defect energetics, and solvus boundaries in the PbTe-$AgSbTe_2$ system

S. V. Barabash,[1] V. Ozolins,[1] and C. Wolverton[2]
[1]*Department of Materials Science and Engineering, University of California–Los Angeles, California 90095-1595, USA*
[2]*Department of Materials Science and Engineering, Northwestern University, Evanston, Illinois 60208, USA*
(Received 26 July 2008; published 22 December 2008)

Using first-principles data for the elastic properties of PbTe, $AgSbTe_2$, and related compounds, we extend our previous theoretical study of the thermodynamics of PbTe-$AgSbTe_2$ and present an in-depth analysis of the effects of elastic strain on the thermodynamics of ordering and coherent solvus boundaries. We find that the substitutional site preference for Pb in ordered $AgSbTe_2$ and the large asymmetry of the PbTe-$AgSbTe_2$ miscibility gap share a common physical origin in the peculiar defect energetics of $AgSbTe_2$. In particular, we find that Pb substitution on Ag sites has approximately the same energy cost as a complex defect consisting of Pb substitution on an Sb site combined with an Sb_{Ag} antisite defect. Configurational entropy contributions strongly favor the latter, explaining why Pb substitutes almost exclusively on the Sb sites in $AgSbTe_2$. Coherency strain is shown to increase the solubility limits by a factor of ~2 relative to the bulk values both for Ag,Sb in PbTe and for Pb in $AgSbTe_2$.

DOI: 10.1103/PhysRevB.78.214109 PACS number(s): 64.70.kg, 61.66.Fn, 63.20.dk, 64.75.Qr

I. INTRODUCTION

Recently, a high thermoelectric figure of merit $ZT \sim 2$ (at $T=800$ K) has been observed in bulk inhomogeneous $AgPb_mSbTe_{2+m}$ alloys.[1] While these measurements have demonstrated the exciting promise of these materials for thermoelectric power generation, they have also underscored the current lack of understanding of the structure and phase stability of lead-antimony-silver-telluride (LAST) alloys. Indeed, contradictory experimental assessments have been made for the isoplethal PbTe-$AgSbTe_2$ section of the phase diagram: full miscibility[2–4] and a miscibility gap[5] between rocksalt PbTe and $AgSbTe_2$ have both been reported, with the $AgSbTe_2$ compound found to either have a disordered (Ag,Sb) cation sublattice[6] or to exhibit signs of cation order.[7] However, recent work has begun to clarify these issues: strong evidence for the existence of a miscibility gap (at least away from the isoplethal PbTe-$AgSbTe_2$ section) has been found in recent measurements.[1,7–9] First-principles calculations were able to identify[10,11] the type of cation ordering in $AgSbTe_2$, and, recently, we investigated[11] the thermodynamics of the solid Pb-Ag-Sb-Te alloy system from first-principles density-functional theory (DFT) calculations. As shown in Fig. 1(a), we found that the isoplethal PbTe-$AgSbTe_2$ section of the phase diagram exhibits a highly asymmetric miscibility gap between the binary PbTe and the ordered ternary $AgSbTe_2$ phases, with miscibility limits of ~0.6% (for Ag,Sb in PbTe) vs ~8% (for Pb in $AgSbTe_2$) at $T=850$ K. We also found that $AgSbTe_2$ (which we predicted to remain ordered up to the experimental melting temperature) exhibits a strong Pb substitutional preference for Sb sites, as can be seen from the composition profile shown in Fig. 1(b).

The physical origin of the strong Pb site preference and the asymmetry of the miscibility gap were not given a detailed analysis in Ref. 11. Furthermore, the approach of Ref. 11 did not give an explicit account for the strain interactions that appear in a coherent phase-separating system and their effect on the *coherent* solvus boundaries. Here, we analyze the elastic properties of PbTe, ordered $AgSbTe_2$, and related compounds. Using these data, we extend the investigation of Ref. 11 by analyzing the effects of strain on atomic ordering.

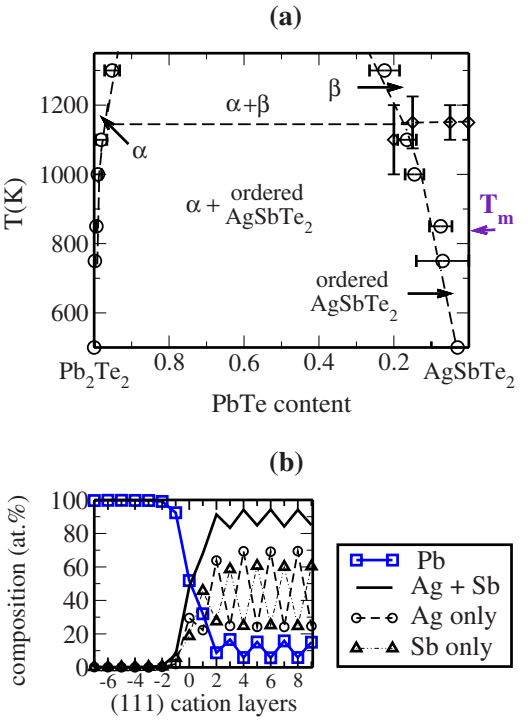

FIG. 1. (Color online) (a) Solid-state phase diagram of rocksalt-based $(PbTe)_{1-x}(AgSbTe_2)_{x/2}$, as calculated in Ref. 11, showing the boundaries of the immiscible disordered α and β solid solution phases (circles) and the order-disorder transition temperature T_{ord} for the ordered $AgSbTe_2$ phase (diamonds). Also marked is the experimental melting temperatures T_m of pure bulk $AgSbTe_2$. (b) Variation in the atomic composition of (111) cation layers in the vicinity of a (111) boundary between PbTe (negative positions) and ordered $AgSbTe_2$ (positive positions), as calculated in Ref. 11. Within the $AgSbTe_2$ phase, Pb has a strong preference for the Sb sublattice.

We further identify the physical origin for the Pb substitutional site preference and for the asymmetry of the miscibility gap which, as we show, are both related to the peculiar energetics of various substitutional and antisite defects in $AgSbTe_2$.

The rest of the paper is organized as follows. In Sec. II, we present our first-principles results for the elastic properties of select LAST structures (in Sec. II A, for pure PbTe and ordered $AgSbTe_2$, and in Sec. II B, for hypothetical rocksalt SbTe and AgTe); we find that strain deformations do not alter the ordering energetics and that the universal softness of (111) direction can be related to the selection of the ordering type in $AgSbTe_2$. In Sec. III, we analyze the peculiar substitutional defect energetics in PbTe and $AgSbTe_2$ and develop a simple model for the resulting entropy contributions, which explains the Pb substitutional site preference and the asymmetry of the miscibility gap in the absence of strain interactions. In Sec. IV, we combine the results of the preceding sections to analyze the effect of coherency strain on the miscibility gap; we find that, in a coherently precipitating system, the solubility limits inside both the precipitates and the matrix are substantially increased relative to the unstrained bulk values (roughly to ~1% for the Ag,Sb solubility in PbTe vs ~15% for the Pb solubility in $AgSbTe_2$). The summary is presented in Sec. V.

II. ELASTIC PROPERTIES OF LAST STRUCTURES

The DFT calculations of the deformation energies were performed in the scalar-relativistic local-density approximation (LDA) (Ref. 12) to the DFT (Ref. 13) using projector-augmented wave potentials[14] as implemented in the VASP code.[15] The spin-orbit corrections have only a small effect on the energy differences between similar (Ag,Pb,Sb)Te structures, as we discussed earlier in Refs. 11 and 16: for example, they change the energy difference between the two ordered $AgSbTe_2$ structures, $L1_1$ and $D4$, by only 0.6 meV/cation.[16] The effect of the generalized-gradient corrections is likewise small.[16] All the relevant total-energy differences were numerically converged to approximately 1 meV/cation. The convergence of the deformation energies was established by comparing calculations with a basis set energy cutoff $E_{cut}=300$ eV and k meshes of $\sim 5000/N_{atoms}$ k-points in the first Brillouin zone to those with $E_{cut}=350$ eV and $\sim 16\,000/N_{atoms}$ k-points (here N_{atoms} is the number of atoms in the supercell). Gaussian smearing of 0.1 eV was used for relaxation runs, and the highly accurate tetrahedron method with Blöchl corrections was used for all the calculations in the final relaxed geometries and for the epitaxial calculations. For the epitaxial calculations, the uniaxial deformation parameter (the c/a ratio) and the cell-internal atomic positions were optimized for each value of the in-plane lattice constant (defined by uniformly expanding or contracting the specified atomic plane), and the resulting total energy per cation, minus the total energy of the unstrained material, was defined as a deformation energy.

A. PbTe/$AgSbTe_2$ system

We calculated the elastic deformation energies of pure PbTe and two fully ordered pure $AgSbTe_2$ structures with

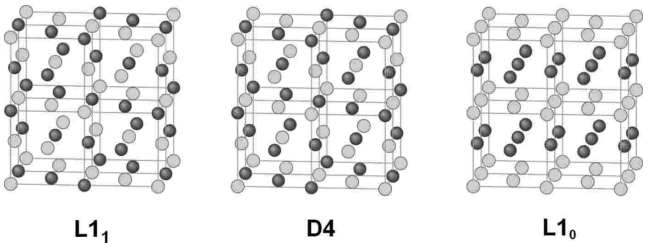

FIG. 2. Different types of ordering of Ag and Sb on the cation sublattice of $AgSbTe_2$: the trigonal $L1_1$ and cubic $D4$ are the nearly degenerate ground states found in Refs. 10 and 11; $L1_0$ is used here for comparison. For visual clarity, the Te sublattice (the anion sublattice of the underlying rocksalt lattice) is not shown.

$L1_1$ and $L1_0$ cation orderings under both hydrostatic and epitaxial strains. Figure 2 shows the ordered $L1_1$ and $L1_0$ structures, as well as the predicted $D4$ ground-state structure of $AgSbTe_2$, which is closely related to $L1_1$. Structures $L1_1$ and $D4$ were identified in Refs. 10 and 11 as nearly degenerate cation ordering types in $AgSbTe_2$ while $L1_0$ has a considerably higher energy and is included here for comparison. The two lowest-energy structures $L1_1$ and $D4$ possess strong structural similarities:[17] for instance, the number of like and unlike neighbor ions with *any* given separation is identical for both structures; similarly the average three-body correlations are all equal. [Here a three-body correlation function corresponding to a triplet cluster f is the sum $\Pi_f=\Sigma_{n=0}^{3}(-1)^n N_f(Ag_{3-n}Sb_n)$, where $N_f(Ag_{3-n}Sb_n)$ is the number of Ag_nSb_{3-n} triplets per lattice site and f refers to all the instances of a given geometric combination of ideal lattice sites (e.g., a triangle formed by three nearest-neighbor atoms within fcc). This definition naturally appears within the cluster-expansion approaches (see Refs. 16–18 for further discussion).] We thus used the smaller-size $L1_1$ for our elastic calculations[19] (the small deviation of the planar geometry of $L1_1$ from that of cubic structures was fixed to the unstrained value). We found that the deformation energies for the orientations made inequivalent by the trigonality in $L1_1$ [e.g., for (111) vs $(\bar{1}11)$ epitaxial planes] agree within 3 meV/cation. To visualize the relative effect of strain on the constituents, we further define the coherent strain energy E_{cs} as the energy of infinite-period A/B (e.g., $AgSbTe_2$/PbTe) superlattices at a fixed composition x, i.e., $(A)_{N(1-x)}(B)_{Nx}$ as $N\to\infty$,

$$E_{CS}=\min_{a_\perp\in(a_A,a_B)}[(1-x)E_{strain}(A,\hat{k},a_\perp)+xE_{strain}(B,\hat{k},a_\perp)], \tag{1}$$

where $E_{strain}(A,\hat{k},a_\perp)=E(A,\hat{k},a_\perp)-E(A,a_A)$ is the epitaxial strain energy[20] of material A deformed along direction $\hat{k}$ in such a way that the in-plane lattice constant is given by $a_\perp$ (taken relative to the undeformed energy of the same material A at its own equilibrium lattice constant a_A).

We find that PbTe is generally harder than $AgSbTe_2$ and that in both PbTe and $AgSbTe_2$ the softest direction is (111) and the hardest is (100). This is illustrated in Fig. 3, where we plot the strain energies of infinite-period PbTe/$AgSbTe_2$

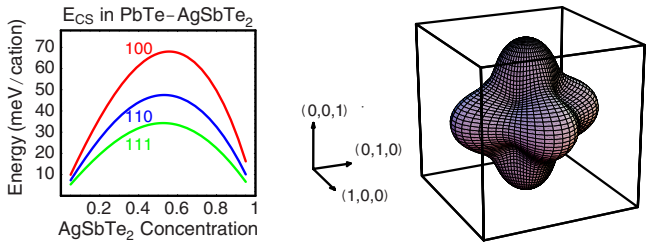

FIG. 3. (Color online) The strain energy of infinite-period $N\rightarrow\infty$ superlattices $(AgSbTe_2)_{N(1-x)}(PbTe)_{Nx}$ as a function of net composition x for selected orientations of superlattice interfaces (left), and the interpolated direction dependence of the strain energy at $x=0.5$ (right).

superlattices in selected directions as functions of the total composition, together with the interpolated directional dependence of the strain energy for equal-period $PbTe/AgSbTe_2$ superlattices (the interpolation was performed using Kubic harmonic functions[21]). This hardness of (100) and the softness of (111) directions is generally expected from the rocksalt structures, which have bonds parallel to [100] direction.[22] In Fig. 4, we plot the epitaxial strain energies along the softest and the hardest directions, as well as the hydrostatic strain energy. We see that, in particular, the energy difference between the two different ordered $AgSbTe_2$ structures (the solid and the dotted blue curves) is largely unaffected by the strain. Furthermore, in a separate calculation, we found that even the small energy difference (1.7 meV/cation) between the competing ground-state structures $L1_1$ and $D4$ is not affected by the coherency strain from PbTe matrix: restricting the c/a ratio of the $L1_1$ structure to the ideal cubic rocksalt value and distorting both $L1_1$ and $D4$ to the lattice constant of PbTe still yields the same 1.7 meV difference in favor of $D4$. We therefore conclude that the strain has negligible effects on the type and relative energetics of cation ordering *at a fixed composition*. However, as will be shown in Sec. IV, the strain will affect the *compositions* of coherently coexisting immiscible phases.

In Table I, we present the calculated elastic parameters of PbTe and $AgSbTe_2$. Note that, for an anisotropic material, Poisson's ratio (defined as $\nu=-\varepsilon_{xx}/\varepsilon_{zz}$, the ratio of the in-plane to out-of-plane strain under a fixed *uniaxial* strain ε_{zz}) not only depends on the deformation direction but also takes different values for different transverse directions.[22,23] Here we first define a similar ratio $f=-\varepsilon_{xx}/\varepsilon_{zz}$ under a fixed *epitaxial* in-plane strain $\varepsilon_{xx}=\varepsilon_{yy}$ and then use it to define an "effective" Poisson's ratio via the isotropic-case relationship $f=(1-\nu)/2\nu$. We see from Fig. 3 and Table I that there is a considerable anisotropy in the elastic properties of both PbTe and $AgSbTe_2$. Also, by fitting the first-principles data to fourth-order polynomials, we find that nonlinear contributions to the elastic energies in Fig. 4 constitute over 30% for some points. In principle, a rigorous treatment of the elastic strain in a coherent $PbTe/AgSbTe_2$ system would thus require a general solution of a problem in an anisotropic nonlinear elastic system, which in turn would require determination of all the linear and nonlinear elastic constants far beyond the basic analysis presented in Table I. For our study of the effect of the strain on the compositions of coherent phases, we did not attempt to perform such an exhaustive analysis. Instead, we approximated the complicated inhomogeneous strain effects by a simple model of an isotropic spherical inclusion in an isotropic environment with similar elastic moduli, using linear elasticity theory with a Poisson ratio $\nu\approx 1/3$ (which gives a reasonable approximation to the effective ν values in Table I).

B. Rocksalt AgTe/SbTe system

The energetic preference for $L1_1$ $AgSbTe_2$ over $L1_0$ $AgSbTe_2$ can be related to the underlying strain energetics of hypothetical AgTe and SbTe phases with the rocksalt structure. The process of forming ordered short-period superlattices (such as $L1_1$ and $L1_0$) from these rocksalt phases can be broken down into two steps. In the first step, rocksalt AgTe and SbTe are epitaxially deformed in the (111) [or (100)] plane to a common lattice constant. In the second step, ordered short-period $(AgTe)_1(SbTe)_1$ superlattices along the [111] ([100]) direction are formed to obtain ordered $L1_1$ ($L1_0$). The elastic deformation energy associated with the first step is offset by interfacial energy gain in the second step due to fully satisfying the chemical charge balance between the preferred Ag^{1+}, Sb^{3+}, and Te^{2-} ionic states of the constituent elements. We find that (111) is again the softest direction in both AgTe and SbTe. Moreover, as we illustrate

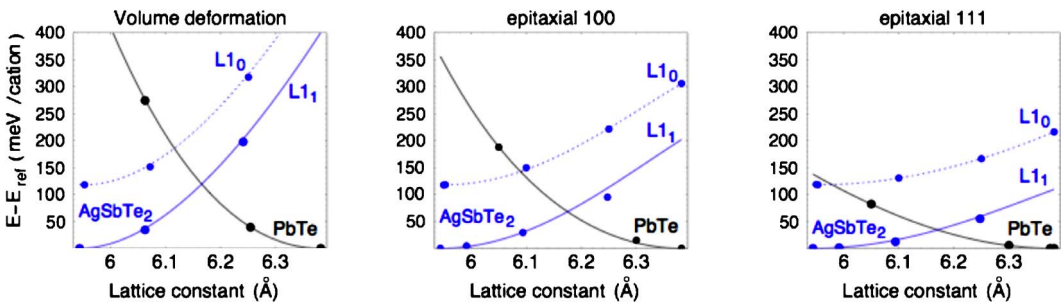

FIG. 4. (Color online) Energies of PbTe (black) and of $AgSbTe_2$ with $L1_1$ (blue solid line) and $L1_0$ (blue dotted line) cation ordering vs in-plane lattice constant under epitaxial or hydrostatic ("volume") deformations (as indicated above the individual plots), relative to the energies of the unstrained PbTe and of $L1_1$-ordered $AgSbTe_2$. The lines are the fourth-order fits to the data (more data was used for fitting than actually shown). For the trigonal $L1_1$ structure, the epitaxial energies for the nonequivalent (111) and (−111) directions differ by less than 2 meV/cation.

TABLE I. Elastic constants of PbTe and $L1_1$-ordered $AgSbTe_2$ as given by LDA: the lattice parameter a, the bulk modulus B, the ratio of the in-plane to out-of-plane strain under an epitaxial load f (for different directions), and the corresponding "effective Poisson ratio" $\nu(f)$ (the same ratio under a uniaxial load), as defined in the text. [The error in ν corresponds to the numerical fit error for f (not shown); for the nonequivalent directions in trigonal $AgSbTe_2$, the values of f corresponding to both directions are given and the difference is included into the error in ν.]

	PbTe				$L1_1$-ordered $AgSbTe_2$			
Deformation direction	a (Å)	B (10^{10}N m^{-2})	f	ν	a (Å)	B (10^{10}N m^{-2})	f	ν
bulk	6.38	5.0			5.94	6.8		
(001)			3.5	0.13 ± 0.02			2.5	0.16 ± 0.03
(110)			1.08	0.32 ± 0.02			1.03–1.08	0.32 ± 0.03
(111)			0.76	0.40 ± 0.01			0.80–0.82	0.38 ± 0.01

in Fig. 5, this direction is particularly soft in rocksalt SbTe. Even though no imaginary frequencies in the calculated phonon spectrum[24] were found, the material appears to be on the verge of instability. Indeed, epitaxially strained SbTe adopts changes of the in-plane lattice constant $a_\perp$ ranging from 5.8 to 6.4 Å with a corresponding energy change of only a few meV/cation, as seen in the left panel of Fig. 5. Therefore, creating the $L1_1$-ordered $AgSbTe_2$ [a (111) based superlattice] via the above two-step process requires negligible elastic energy penalty, compared to ~100 meV/cation penalty for the (100) superlattice structure $L1_0$, while gaining a similar amount of chemical energy by fully satisfying the charge balance requirements. While the formation of $D4$ cannot be given a simple superlattice interpretation, within the reciprocal-space constituent strain formalism[25] the strain contribution to the formation energy of $D4$ is expected to be exactly the same as for $L1_1$ (Ref. 26) due to the identical values of pair-correlation functions in these structures. These intuitive considerations agree very well with the actual energy differences between fully relaxed $D4$, $L1_1$, and $L1_0$ $AgSbTe_2$ structures.

III. SUBSTITUTIONAL DEFECT ENERGETICS AND THE PHASE DIAGRAM IN THE ABSENCE OF STRAIN

Here we analyze the effects that are responsible for the peculiar site preference of substitutional Pb in $AgSbTe_2$ and the asymmetry of the miscibility gap in the PbTe-$AgSbTe_2$ system and show that these effects stem from the interplay between the energies of the substitutional defects in PbTe and $AgSbTe_2$. Table II summarizes our directly calculated LDA values of the formation energies of key defects, as well as the values predicted by the cluster expansion (CE) of Ref. 11. [For consistency with Ref. 11, the defect energies are expressed in terms of the formation energy differences; in turn, the formation energy of a $Pb_{1-x-y}Ag_ySb_xTe$ structure σ is defined with respect to the pure rocksalt tellurides as $\Delta H(\sigma) = E_{tot}(\sigma) - (1-x-y)E_{tot}(PbTe) - xE_{tot}(AgTe) - yE_{tot}(SbTe)$, where both E_{tot} and ΔH are per cation site.]

Table II shows that Pb substitution on a Ag site (Pb_{Ag} defect) in $D4$-ordered $AgSbTe_2$ has a very high energetic cost in comparison with other substitutional (Pb_{Sb}) and antisite (Ag_{Sb}, Sb_{Ag}) defects. In the cluster expansion of Ref. 11, this was reflected by a largeness of the three-body interactions, which are generally known to lead to an asymmetry in the phase diagram. However, in the case of LAST alloys, the predicted asymmetry in the solubility limits can be explained on a deeper physical level. In particular, the data in Table II show that the cost of Pb_{Ag} in the $AgSbTe_2$ phase [$\Delta E(Pb_{Ag}) = 0.73$ eV] is nearly the same as the net cost of $Pb_{Sb} + Sb_{Ag}$ "complex defect" [$\Delta E(Pb_{Sb}) + \Delta E(Sb_{Ag}) = 0.76$ eV]. We show below that the latter complex defect gives a larger contribution to the configurational entropy and

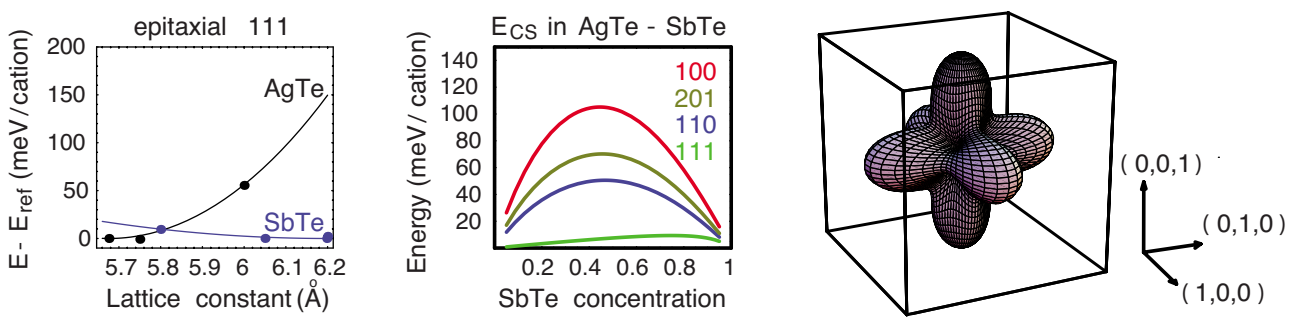

FIG. 5. (Color online) Left: Deformation energies of rocksalt AgTe (black) and of hypothetical rocksalt SbTe (blue) vs in-plane lattice constant under (111) epitaxial deformation. Center: the strain energy of infinite-period $N \to \infty$ superlattices $(AgTe)_{N(1-x)}(SbTe)_{Nx}$ as a function of net composition x for selected orientations of superlattice interfaces. Right: the interpolated direction dependence of the strain energy of the infinite-period AgTe/SbTe superlattices at the equiatomic composition.

TABLE II. Comparison of cation substitution defect energies in $D4$-ordered $AgSbTe_2$ and PbTe, as given by LDA calculations in a 16-atom supercell and by a CE. Here A_B means that A impurity occupies the lattice site that, in the absence of the defect, is occupied by B.

Reference compound	Defect	$\Delta E^{\mathrm{LDA}}=[\Delta H^{\mathrm{LDA}}(\mathrm{defect})-\Delta H^{\mathrm{LDA}}$ (reference)] (meV/defect)	$\Delta E^{\mathrm{CE}}=[\Delta H^{\mathrm{CE}}(\mathrm{defect})-\Delta H^{\mathrm{CE}}$ (reference)] (meV/defect)
$D4$	Ag_{Sb}	343.8	287.3
	Sb_{Ag}	364.3	270.2
	Pb_{Sb}	392.9	282.0
	Pb_{Ag}	727.1	550.0
PbTe	Ag_{Pb}	637.1	476.0
	Sb_{Pb}	402.8	381.0

is therefore expected to dominate at sufficiently high temperatures.

We next use a mean-field ideal solution approximation[27] to estimate the entropy associated with Pb substitutional defects in $AgSbTe_2$. We consider an ordered $AgSbTe_2$ with a 1:1 ratio of Ag and Sb, assuming a total of N cation sites, of which xN sites are substitutionally alloyed by Pb. We first consider the case for which Pb is uniformly distributed between Ag and Sb sites, and alternatively the case for which Pb is preferentially distributed on Sb sites.

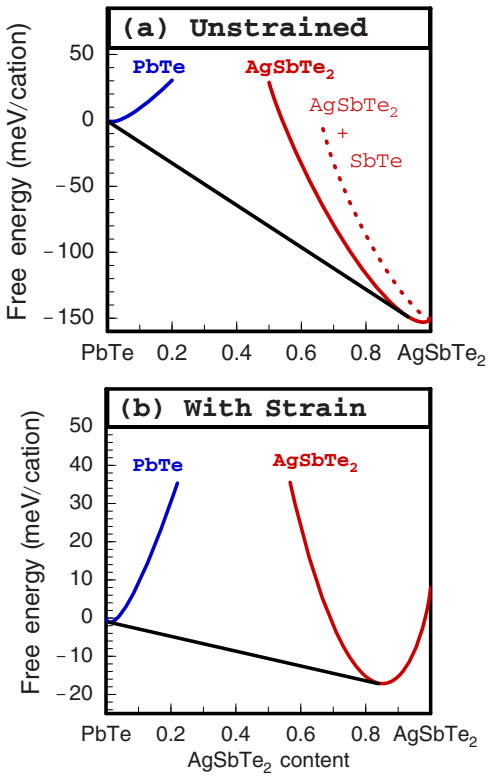

FIG. 6. (Color online) Model free energies of PbTe (blue) and $AgSbTe_2$ (red) phases as a function of composition, for different cases of strain distribution, at $T=850$ K. Black lines show common-tangent constructions. (a) Unstrained bulk phases (solid lines) in the absence of strain: solubility limits are 0.2% vs 7%. The dashed red line corresponds to a hypothetical alternative model for Pb-doped $AgSbTe_2$ as discussed in the text (displaced Sb separating as rocksalt SbTe, instead of moving to antisites). (b) Coherent (strained) $AgSbTe_2$ precipitates inside PbTe matrix. The strain increases the solubility limits to 1% vs 16%.

Uniform distribution of Pb on Ag/Sb sites. If the defect energies were the same for Pb substitution on Ag and Sb sites [or, generally, if one had $\Delta E(\mathrm{Pb_{Ag}}) \ll \Delta E(\mathrm{Pb_{Sb}})+\Delta E(\mathrm{Sb_{Ag}})$ and $\Delta E(\mathrm{Pb_{Sb}}) \ll \Delta E(\mathrm{Pb_{Ag}})+\Delta E(\mathrm{Ag_{Sb}})$], Pb atoms would be distributed uniformly between the Ag and Sb sublattices of the ordered $AgSbTe_2$ phase. In this scenario, $xN/2$ sites in each of the Ag and Sb sublattices would be occupied by Pb, and $(1-x)N/2$ sites would be occupied by Ag and Sb each, yielding the following mean-field expression for the configurational entropy of mixing in the ideal solution approximation:

$$S^0_{\mathrm{AgSbTe_2}} = -k_B N[x \ln x + (1-x)\ln(1-x)]. \tag{2}$$

Preferential distribution of Pb on Sb sites. On the other hand, if one assumes that a total number xN of Pb atoms occupy exclusively the $N/2$ sites of the Sb sublattice, and $xN/2$ Sb atoms create antisites within the Ag sublattice to preserve the 1:1 ratio of Ag to Sb, then the mean-field mixing entropy is

$$S'_{\mathrm{AgSbTe_2}} = -k_B N/2[2x \ln(2x) + x \ln x + (1-2x)\ln(1-2x) + (1-x)\ln(1-x)]. \tag{3}$$

Note that as long as $x<1/3$, $S'_{\mathrm{AgSbTe_2}} > S^0_{\mathrm{AgSbTe_2}}$. Furthermore, the entropy can be shown to increase monotonously between these two limiting cases, as the fraction of Pb atoms occupying the Ag sublattice is changed from $\frac{1}{2}$ to 0. Thus, at $T \gg |\Delta E(\mathrm{Pb_{Ag}})-\Delta E(\mathrm{Pb_{Sb}})-\Delta E(\mathrm{Sb_{Ag}})|/k_B \sim 300$ K, Pb-doped $AgSbTe_2$ acquires additional entropy by creating Sb_{Ag} antisites necessary to accept all Pb within the Sb sublattice. This simple model explains the Monte Carlo (MC) results of Ref. 11, which found that for 11% Pb-doped $AgSbTe_2$ at $T=750$ K, the vast majority of substitutional Pb atoms (92%) occupied the Sb sublattice [cf. Fig. 1(b)].

This additional entropy predicted by this simple mean-field model can also be used to rationalize the asymmetry of the miscibility gap in the calculated phase diagram [cf. Fig. 1(a)]. The entropy of Ag,Sb-doped PbTe with $yN=(1-x)N$ cation sites occupied by Ag and Sb (here $y=1-x$, and it is assumed that Ag and Sb each occupy half of the yN sites) is given by

$$S_{\mathrm{PbTe}} = -k_B N[y \ln y + (1-y)\ln(1-y)] - k_B(yN)\left[\frac{1}{2}\ln\left(\frac{1}{2}\right) + \frac{1}{2}\ln\left(\frac{1}{2}\right)\right]. \quad (4)$$

Neglecting the possible imbalance of Ag and Sb content and using the above expressions for $S'_{\mathrm{AgSbTe_2}}$ and S_{PbTe}, as well as the energies obtained from the CE of Ref. 11 (listed in Table II), the free energies of the doped phases can be estimated, as illustrated by the solid lines in Fig. 6(a). A common-tangent construction yields strongly asymmetric solubility limits of 0.2% for Ag,Sb in PbTe and 7% for Pb in $AgSbTe_2$ at 850 K, in close agreement with the results of our detailed MC study.

In the discussion above, we assumed that the entropy gain given by Eq. (3) is sufficient to overcome the energetic cost of creating Sb_{Ag} antisites. The dashed red line in Fig. 6(a) represents an alternative scenario in which the displaced Sb phase is assumed to phase separate as a separate rocksalt SbTe phase; indeed, we see that this scenario is energetically unfavorable.

We note in passing that using the defect energetics obtained from direct LDA supercell calculations (see Table II) instead of the CE-predicted energies yields a similar asymmetry but smaller solubility limits: 0.1% and 2%, respectively. This may in fact indicate that the CE of Ref. 11 overestimates the solubility limits due to underestimating the defect energies (cf. Table II). We found, however, that refitting the CE using the additional LDA energies of isolated defects results in a better agreement between the LDA and CE energies for the isolated defects listed in Table II but gives very little change in the miscibility limits at $T=850$ K. It is thus possible that the energetics of more complex defects, described by the CE but neglected in the above model, affects the actual values of the miscibility limits.

IV. EFFECT OF STRAIN ON PHASE EQUILIBRIA

We now combine the results obtained in Secs. II and III to evaluate the effect of the coherency strain on the compositions and coherent solvus boundaries of the immiscible coherent phases, compared to those shown in the unstrained (*bulk*) phase diagram of Fig. 1(a). Neglecting elastic anisotropy, difference in the elastic constants of the precipitate and the matrix, and size-dependent contributions from the interfacial energy,[28] the contribution ΔF_{el} to the free energy due to a coherent matching of a precipitate of volume V to the matrix is

$$\Delta F_{\mathrm{el}} = VE\varepsilon^2/(1-\nu), \quad (5)$$

where ε is the lattice mismatch, E is Young's modulus and ν is the Poisson ratio. Using Vegard's law, the variation in the mismatch ε with the Pb content x in $AgSbTe_2$ can be approximated as $\varepsilon(x)=x(a_{\mathrm{AgSbTe_2}}-a_{\mathrm{PbTe}})/a_{\mathrm{av}}$, where $a_{\mathrm{AgSbTe_2}}$ and a_{PbTe} are the unstrained lattice constants and $a_{\mathrm{av}}=(a_{\mathrm{AgSbTe_2}}+a_{\mathrm{PbTe}})/2$. Assuming that the volume of the PbTe matrix is much greater than the net volume of the $AgSbTe_2$ precipitates and taking into account the low solubility of Ag and Sb, the effect of changing composition of PbTe on ε can be neglected.

Combining Eq. (5) with mean-field expressions (3) and (4) for the entropy, we obtain the model free-energy curves shown in Fig. 6(b). Comparing these results with the incoherent free energies in Fig. 5(a), we see that, within the same entropy model, the elastic strain increases the coherent solubility of Pb in $AgSbTe_2$ from 7% to 16%, and the solubility of (Ag,Sb) in PbTe from 0.2% to 1%. Note that the actual coherent solubility limits may, however, be smaller due to the above-noted underestimate of the isolated defect energies in the CE.

A similar model can be applied to PbTe precipitates inside a $AgSbTe_2$ matrix, yielding the same numerical results. However, in the case of PbTe precipitates, this simple model overestimates the effect of strain. Indeed, due to the large solubility of Pb in the $AgSbTe_2$ matrix, the strain around the precipitates will locally increase the content of Pb in the matrix, which in turn will partially relieve the strain (both inside the matrix and in the precipitate), and will further lower the free energy by raising the entropy of Pb solute in the matrix. We did not attempt to estimate the magnitude of such a strain relief, as it may be less pronounced than the other effects neglected in our simple model.

V. CONCLUSIONS

In conclusion, we have calculated the energetics of elastic deformations and substitutional defects for ordered LAST structures. We demonstrate that the coherency strain in phase-separating PbTe-$AgSbTe_2$ alloys considerably increases the *coherent* solubility limits in comparison with the unstrained bulk limits found in Ref. 11 [at $T=850$ K, the (Ag,Sb) solubility in PbTe is increased to roughly $\sim 1\%$, and the Pb solubility in ordered $AgSbTe_2$ is increased to roughly $\sim 15\%$]. We also conclude that the strain deformations do not alter the ordering energetics and demonstrate that the $L1_1/D4$ ordering predicted[10,11] for $AgSbTe_2$ can be related to the elastic softness of rocksalt SbTe and AgTe/SbTe superlattices with respect to epitaxial deformations in the (111) lattice plane.

ACKNOWLEDGMENTS

The authors gratefully acknowledge financial support from NSF under Grants No. DMR-0427638 (S.V.B. and V.O.) and No. CBET-0730929 (C.W.) and from the FCRP Focus Center for Functional Engineered Nano Architectonics (S.V.B. and V.O.). The calculations in this research were in part supported by the NSF through TeraGrid resources provided by SDSC and NCSA.

[1] K. F. Hsu, S. Loo, F. Guo, W. Chen, J. S. Dyck, C. Uher, T. Hogan, E. K. Polychroniadis, and M. G. Kanatzidis, Science **303**, 818 (2004).
[2] H. Fleischmann, Z. Naturforsch. B **16a**, 765 (1961), in German.
[3] L. Borisova, S. Decheva, S. Dimitrova, and P. Moraliiskii, Annual of Sofia University **65**, 167 (1971); L. Borisova and S. Dimitrova, Phys. Status Solidi A **53**, 403 (1979); L. Borisova, Phys. Status Solidi B **126**, K155 (1984).
[4] R. G. Maier, Z. Metallkd. **54**, 311 (1963), in German.
[5] H. Rodot, Compt. Rend. **249**, 1872 (1959), in French.
[6] S. Geller and J. H. Wenick, Acta Crystallogr. **12**, 46 (1959).
[7] E. Quarez, K. F. Hsu, R. Pcionek, N. Frangis, E. K. Polychroniadis, and M. G. Kanatzidis, J. Am. Chem. Soc. **127**, 9177 (2005).
[8] N. Chen, F. Gascoin, and G. J. Snyder, Appl. Phys. Lett. **87**, 171903 (2005).
[9] H. Lin, E. S. Bozin, S. J. L. Billinge, E. Quarez, and M. G. Kanatzidis, Phys. Rev. B **72**, 174113 (2005).
[10] K. Hoang, S. D. Mahanti, J. R. Salvador, and M. G. Kanatzidis, Phys. Rev. Lett. **99**, 156403 (2007).
[11] S. V. Barabash, V. Ozolins, and C. Wolverton, Phys. Rev. Lett. **101**, 155704 (2008).
[12] D. M. Ceperley and B. J. Alder, Phys. Rev. Lett. **45**, 566 (1980); J. P. Perdew and A. Zunger, Phys. Rev. B **23**, 5048 (1981).
[13] P. Hohenberg and W. Kohn, Phys. Rev. **136**, B864 (1964); W. Kohn and L. J. Sham, *ibid.* **140**, A1133 (1965).
[14] P. E. Blöchl, Phys. Rev. B **50**, 17953 (1994); G. Kresse and D. Joubert, *ibid.* **59**, 1758 (1999).
[15] G. Kresse and J. Hafner, Phys. Rev. B **48**, 13115 (1993); G. Kresse and J. Furthmüller, Comput. Mater. Sci. **6**, 15 (1996); Phys. Rev. B **54**, 11169 (1996).
[16] See Ref. 11, especially EPAPS Document No. E-PRLTAO-101-007839. For more information on EPAPS, see http://www.aip.org/pubservs/epaps.html
[17] A. Finel, Ph.D. thesis, University of Paris, 1987; Z. W. Lu, S.-H. Wei, A. Zunger, S. Frota-Pessoa, and L. G. Ferreira, Phys. Rev. B **44**, 512 (1991); C. Wolverton and A. Zunger, J. Electrochem. Soc. **145**, 2424 (1998).
[18] J. M. Sanchez, F. Ducastelle, and D. Gratias, Physica A **128**, 334 (1984).
[19] We also performed an explicit calculation for (111) epitaxial deformation of $D4$ and found that the results agree with the elastic curves fitted to $L1_1$ data within the accuracy of the fit.
[20] See, e.g., J. F. Nye, *Physical Properties of Crystals* (Clarendon, Oxford, 1957).
[21] A. Zunger, L. Wang, G. Hart, and M. Sanati, Modell. Simul. Mater. Sci. Eng. **10**, 685 (2002); V. Ozolins, C. Wolverton, and A. Zunger, Phys. Rev. B **57**, 6427 (1998).
[22] D. J. Bottomley and P. Fons, J. Cryst. Growth **160**, 406 (1996).
[23] A. Ballato, IEEE Trans. Ultrason. Ferroelectr. Freq. Control **43**, 56 (1996).
[24] The calculations were performed with $2\times2\times2$ and $3\times3\times3$ samplings of the Brillouin zone for the phonon q vectors. For the details of the method, see C. Wolverton, V. Ozolins, and M. Asta, Phys. Rev. B **69**, 144109 (2004).
[25] D. B. Laks, L. G. Ferreira, S. Froyen, and A. Zunger, Phys. Rev. B **46**, 12587 (1992); C. Wolverton, V. Ozolins, and A. Zunger, J. Phys.: Condens. Matter **12**, 2749 (2000).
[26] $L1_1$ has a nonzero structure factor $|S(\mathbf{k})|^2=1$ for $\mathbf{k}$ at a single L point of the Brillouin zone while $D4$ has $|S(\mathbf{k})|^2=1/4$ at all the four L points, resulting in the same constituent strain energy within the formalism of Ref. 25.
[27] D. A. Porter and K. E. Easterling, *Phase Transformations in Metals and Alloys* (CRC, Boca Raton, FL, 1992).
[28] M. E. Thompson, C. S. Su, and P. W. Voorhees, Acta Metall. Mater. **42**, 2107 (1994).